

Sea Ice Thickness from Kinematics

R. Kwok and B. Holt
Jet Propulsion Laboratory
California Institute of Technology
MS 300-235
4800 Oak Grove Drive
Pasadena, California 91109
USA

Tel: (818) 354-5614 Fax: (818) 393-3077 email: Ronald.Kwok@jpl.nasa.gov

ABSTRACT

High resolution 3-day surveys of the Arctic Ocean are currently being obtained using the Canadian RADARSAT synthetic aperture radar with its wide-swath ScanSAR mode. For the first time, we can produce basin-scale estimates of sea ice age and thickness from Lagrangian observations of ice motion derived from sequential SAR images of the Arctic Ocean. The deformation of material elements (cells) on the SAR imagery is computed using strain rates from ice motion. From the record of deformation of each cell, we estimate the ice age and thickness. In the winter, open water and thin ice are created when there is a positive change in area while negative area changes are associated with ridging. The deformation of the ice cover is sampled by cells with an initial area of approximately 10 km by 10 km. More than 60,000 of cells are used to cover the entire Arctic Ocean. These geophysical products can be put to a variety of uses: analyzing new ice climatologies, testing ice models or new ideas about sea ice rheology, and for assimilating into sea ice models.

Thus far, we have produced estimates of sea ice deformation, thickness and age from five months of SAR data of the Arctic Ocean (November 1996 through March 1997). These data products are available on a web site at the Jet Propulsion Laboratory (<http://www-radar.jpl.nasa.gov/rgps>). Here, we describe this data set, their use for studies of the sea ice cover and the potential of using ENVISAT to extend these observations into the future.

INTRODUCTION

The scientific goal of remote sensing of the polar regions is to provide data sets to improve our current understanding of the impact of sea ice on climate and to monitor changes in the Arctic Ocean sea ice cover. Interactions between sea-ice, ocean and atmosphere in the polar regions strongly affect the Earth's climate. Sea ice growth, movement and decay affect energy and mass

balance of the polar ocean system. The surface heat and brine fluxes associated with sea-ice growth contribute significantly to convection of the ocean and thermohaline circulation. Snow covered sea-ice reflects most of the incident solar radiation back into space, while fresh water fluxes associated with melting ice serve as stabilizing elements in the circulation of the North Atlantic waters. Processes along the ice margin and coastlines participate in water-mass formation, upwelling, convection sediment transport and other phenomena.

Global climate models project the largest greenhouse warming in the polar regions [e.g. *Kattenberg et al.*, 1996]. The high-latitude sensitivity displayed by existing climate models has been attributed to positive feedbacks involving surface albedo and reduced sea ice extent and thickness [*Ingram et al.*, 1989; *Rind et al.*, 1995]. Recent years have seen significant changes in the sea level pressure in the Arctic (e.g., *Walsh et al.*, 1996). Correspondingly, buoy data and satellite ice motion data from the 1990s indicate a weakened Beaufort Gyre and a migration of the Transpolar Drift Stream [*Rigor*, per. comm., 1999; *Kwok*, 1999] and variability in ice export that is connected to the North Atlantic Oscillation [*Kwok and Rothrock*, 1999]. A decreasing trend in the Arctic Ocean ice extent is observed in satellite passive microwave observations [*Parkinson et al.*, 1999]. Hydrographic data from recent submarine and icebreaker cruises reveal large-scale changes in the structure of the Arctic upper ocean (e.g., *Steele and Boyd* 1998; *Morison et al.*, 1998). In fact, model simulations show regime shifts in the general surface ocean circulation [*Proshutinsky and Johnson*, 1997; *Zhang et al.* 1998] and the circulation of river water [*Maslowski*, per. comm., 1998]. These changes would undoubtedly be reflected in the surface heat and mass balance of the Arctic Ocean. Understanding and modeling these phenomena require information of sea-ice motion, thickness and concentration.

The remote sensing data set described here addresses the requirement of ice motion and ice thickness observations. The technique (described below) utilizes large volumes sequential SAR imagery. From the Lagrangian observations of sea ice motion, we derive

ice age and ice thickness histograms of the thin ice fraction of the ice cover in the winter. In the summer, we also estimate the open water fraction. The time of melt-onset in the spring and freeze-up in the late fall are estimated from changes in backscatter signature of the ice cover.

These algorithms are implemented in the RADARSAT Geophysical Processor System (RGPS) - a system dedicated to the analysis of SAR data of sea ice collected by the Canadian RADARSAT satellite. RADARSAT was launched in November of 1995 into a 24-day repeat cycle. This orbit configuration and the wide swath (500 km) ScanSAR mode allow the repeat coverage of the Arctic Ocean every 3 to 7 days. To support the data needs of the RGPS, we have been using this mode, termed ScanSAR, to acquire repeat coverage of the Arctic Ocean since November of 1996. Over a 24-day repeat cycle of the satellite, we have close to eight observations of the western Arctic Ocean within the Alaska SAR Facility (ASF) Reception mask in Fairbanks, Alaska. The repeat coverage of the Eurasian Basin is less frequent (6-days) due to the additional cost of RADARSAT data down-linked at the Tromsø Satellite Station in Norway. We expect to continue this acquisition process over the life of the RADARSAT mission. The input SAR imagery is processed to a spatial resolution of approximately 100 m by 100 m, and is calibrated and archived at ASF.

MOTION, AGE AND THICKNESS

This new method estimates ice age and thickness from repeated observations of Lagrangian elements or cells of sea ice in sequential SAR imagery [Kwok *et al.*, 1995]. Fig. 1 shows the time series of observations of one cell within a matrix of such cells, strain ellipses describing the deformation, graphs of the history of cell area, and the thin ice coverage within that cell at the end of a 41-day period. Line segments connecting the four vertices of a cell define its boundaries. The drift and deformation of a cell over time are obtained by tracking the displacement of its vertices in the SAR imagery. The motion tracking procedure is described in Kwok *et al.* (1995). The underlying deformation of the cell evolved from a circle on 8 November 1996 through a series of increasingly eccentric ellipses. The steady evolution of the ellipse, or equivalently the nearly monotonic nature of the invariants, are remarkable. This sequence of observations demonstrates that lead ice controls the mechanical behavior through its orientation and yield strength. This orientation dependence gives the ice cover an anisotropic character.

The age histogram of the ice in a cell is computed from the temporal record of area changes. An age histogram

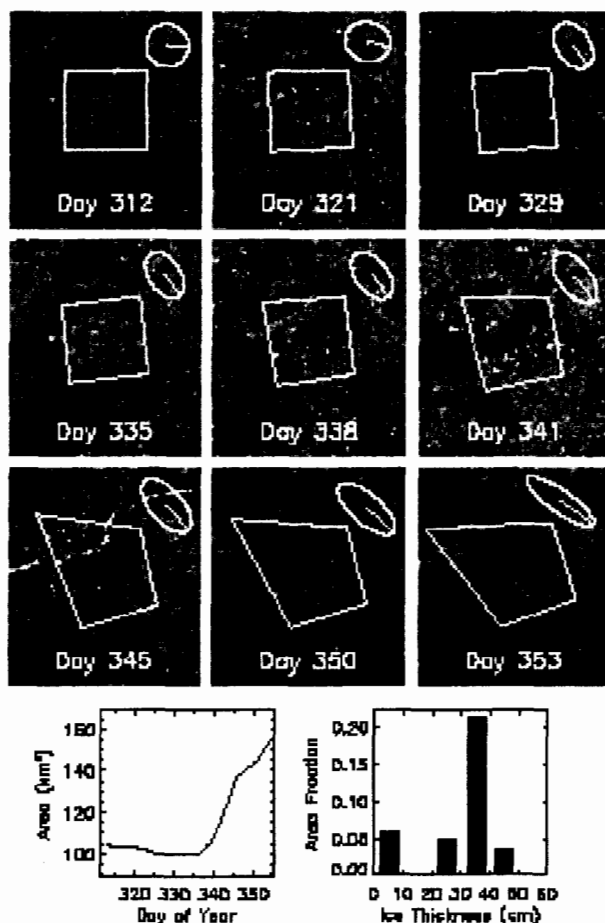


Figure 1. The deformation of a 10 km by 10 km cell over a 41-day period. The record of area changes reflect the opening of the lead running through the cell. The strain ellipses are computed from strain rates.

of sea ice specifies the fractional area covered by ice of different chronological ages. To construct this histogram from sequential observations, we follow the steps below. Every time a new observation is available, we interpret a positive area change as the creation of an area of open water. New ice is assumed to grow over this area immediately after opening. The uncertainty of the ice age occupying this area is dependent on the time interval between observations. This age range is recorded as a new age category in the histogram. At the same time a new category is introduced, existing age categories are 'aged' by the same time interval. In Fig. 1, this procedure created five ice age categories from the sequence of positive area changes since Day 335. A negative change is assumed to have ridged the youngest ice in the cell, reducing its area. The assumption here is that once ridging starts, the deformation tends to be localized in the recently-formed thinner and weaker ice in leads. This area of ridged ice is tracked as a separate category in the age histogram.

Ice age is converted to ice thickness using an empirical ice growth formula. We approximate the growth rate as a function of the number of freezing-degree days (FDD) associated with each age category using Lebedev's parameterization (discussed in *Maykut*, 1986) with $H = 1.33 F^{0.58}$, where H is thickness and F is the accumulated freezing-degree days of that category. Volume is conserved when ice is ridged. We assume that all ridged ice is five times its original thickness and occupies a quarter of the area [*Parmerter and Coon*, 1972].

We start this scheme at fall freeze-up by covering the entire Arctic Ocean with initial 10 km by 10 km square elements, except near the ice margins where 25 km by 25 km are used. Complete coverage of the Arctic takes approximately 70,000 cells. At start up, the ice age/thickness histograms within the cells are unknown. In the process described, the ice volume created over a season is recorded in the thin ice thickness distribution and the ridge volumes. Since we do not melt ice in our scheme, the procedures above work only during the winter ice growth season. The results provide fine age/thickness resolution of only the young/thin end of the age/thickness distributions, but this is the crucial range that produces the most ice growth, the most turbulent heat flux to the atmosphere and the most salt flux to the ocean.

The backscatter intensity of each SAR sample is used to provide an independent estimate of the multiyear (MY) fraction within each cell. The MY algorithm [*Kwok et al.*, 1995] uses a maximum likelihood classifier and a look-up table of expected backscatter characteristics to assign an image pixel to one of two classes: multiyear ice and first-year ice. We assume that the area of MY ice fraction within a cell remains constant throughout the winter (by definition, no multiyear ice is created). Any anomaly in the classification process due to the backscatter variability of other ice types would show up as transients or spikes. These anomalies are filtered out in the time series of MY fraction estimates in each cell.

RGPS DATA PRODUCTS

A brief description of the RGPS data product is given below.

Ice Motion (Lagrangian trajectories). A regular array of points is defined initially on the first image of a long time series of SAR images and an ice tracker finds the positions of those points in all subsequent images of the series. This product contains a record of the trajectories or an array of position measurements of the 'ice particles' that are located on an initial grid which covers the entire Arctic Ocean. The sampling interval is determined by the available repeat coverage of these

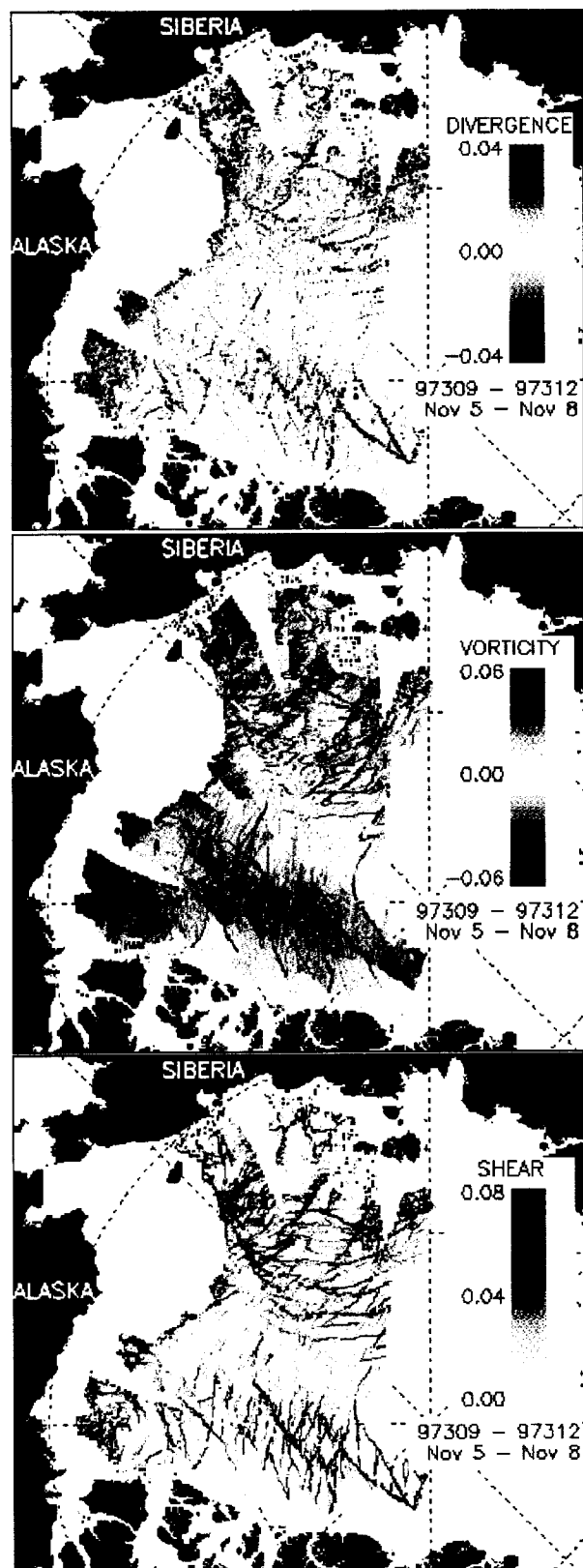


Figure 2. The deformation of the ice cover over three days between Day 309 and 312 in 1997. (a) Divergence. (b) Vorticity. (c) Shear.

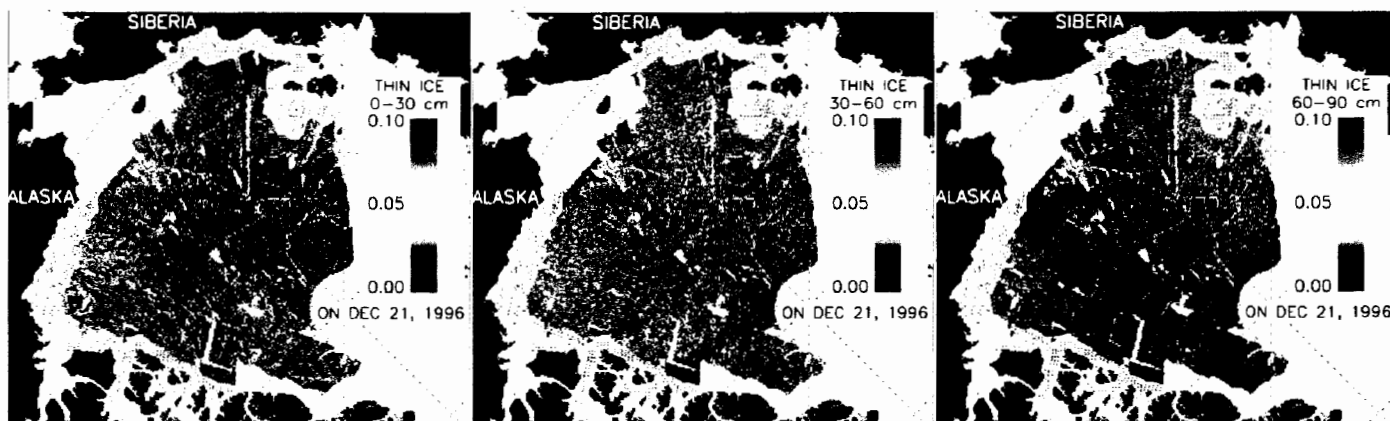


Figure 3. The fractional coverage of thin ice within each grid cell on December 21, 1996.

points by the SAR sensor. The initial grid spacing is 10 km. The accuracy of the position measurements is typically 300m in areas with moderate deformation with higher uncertainties in areas with intense deformation.

Ice Deformation. The local deformation of the ice is computed using the velocity gradients at the vertices of the cells. Fig. 2 shows a basin-scale view of the divergence, vorticity, and shear of the ice cover sampled by the RGPS cells. The deformation fields show linear kinematic features (LKFs) that characterize the opening, closing, and shear of the ice cover.

Ice Age Histogram. The ice age distribution of sea ice specifies the fractional area covered by ice in different age categories as a function of time. This ice age distribution is computed from the field of Lagrangian trajectories described above. The algorithm for determining ice age works only in the winter: the assumption is that there is ice growth in all new leads. It is initialized shortly after fall freeze-up and is operated till the onset of melt. The resolution of age is dependent on the sampling interval of the area of interest. As an example, for a series of images with, say, seven days between successive images, the age classes would be: 0-7 days, 7-14 days, 14-21 days, 21-28 days, ..., first-year ice and multiyear ice. The multiyear ice fraction is obtained with a backscatter-based ice classification algorithm. We keep track of the accumulated freezing-degree days associated with each age class. The surface air temperatures for computing the freezing-degree days are extracted from analyzed air temperature fields. Closings are interpreted as ridging events and the amount of ice that participates in this processes is recorded. This product contains records of local ice age distributions and the accumulated freezing-degree days of each age category within the distributions, and the ridged ice area.

Ice Thickness Histogram. The ice thickness distribution specifies the fractional area covered by ice in different

thickness ranges within a given region as a function of time. The ice thickness distribution is estimated from the ice age distribution using an empirical relationship between the accumulated freezing-degree days and ice thickness. The local age distributions are converted to ice thickness distributions and accumulated over large areas to provide regional scale products; A sampling interval of seven days would cause an uncertainty in the thickness of the thinnest ice of about 23cm (if the air temperature were -20°C) using Lebedev's parameterization (in Maykut, 1986) of the dependence of ice growth on freezing-degree days. Fig. 3 shows the amount of thin ice in different thickness categories on December 21, 1996. The evolution of the basin scale distribution of thin ice thickness and ridged ice can be seen in the histograms in Fig. 4.

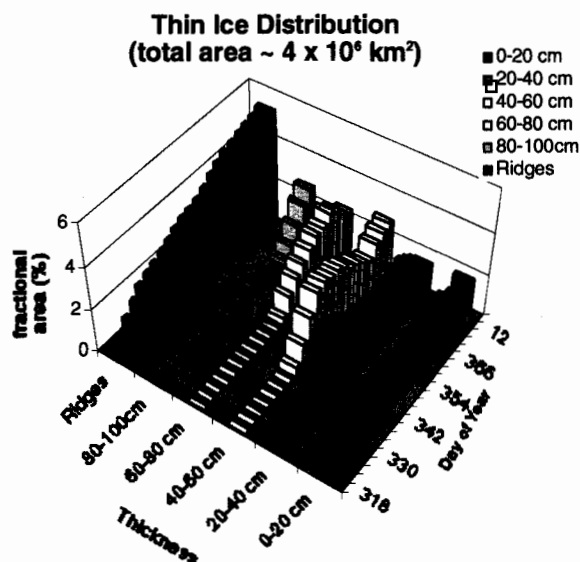


Figure 4. The distribution of thin ice within different thickness ranges and the coverage of ridged ice formed since Day 318.

Open Water Fraction. Summer ice conditions are characterized by an open water fraction. The summer open water fraction in a Lagrangian cell (defined by line segments connecting the tiepoints) is estimated from kinematics and backscatter data.

Backscatter Histogram of Lagrangian cells. The backscatter histograms of the Lagrangian cells are recorded in this product.

Date of Melt-onset in Spring/ Freeze-up in Fall. There is a fairly well-defined change in the backscatter of the snow/ice to the onset of melt and freeze-up. The analysis algorithm will detect and estimate the date this seasonal transition using the time series of backscatter product. Different parts of the Arctic go through these transitions at different dates and this product would provide a high spatial resolution of the date of transition although the temporal resolution is dependent on the repeat observations of the Lagrangian cells.

RGPS STATUS

Status and schedule. Currently the RGPS is processing the winter of 1996/97, which is expected to be completed by December, 1999. With the commissioning of a second operational system this summer, the winter of 1997/98 has been initiated. By the end of year 2000 we expect to have completed both of these winters plus analysis of the summers of 1997 and 1998. We expect to continue to obtain RADARSAT imagery only until November, 2000.

ENVISAT

The RGPS basin-scale products of sea ice age and thickness are truly unique and we anticipate that these data products will have important utility for use in comparisons with climate models and other sensors and data sets. Also, the Arctic is undergoing measurable change this decade in several key indicators of climate warming. The 4-year time record from RADARSAT is fortuitously timed to also potentially provide indicators of climate change through ice motion and age/thickness derivations which are used to determine the surface heat and mass balance of the Arctic Ocean. It therefore seems both desirable and justifiable to continue the unique RGPS derivations over an extended time period. The ENVISAT ASAR wide swath mode presents an excellent opportunity for continued acquisition of high-resolution SAR mapping of the Arctic Ocean. Here we present a brief description of the RGPS requirements and the utility of the ENVISAT ASAR imagery.

In terms of general SAR requirements for the RGPS, repeat wide-swath SAR surveys of the entire Arctic at preferably 3-day near repeat sub-cycles are needed to determine the motion field of the ice cover. Resolution on the order of 100-200 m will resolve moderate deformation and opening/closing of important size-scale of leads. From these, ice age and thickness can be derived over comparatively short time periods. Relative radiometric accuracy of 1 dB or less across the swath provides adequate stability needed for maintaining high areal correlation of ice features between successive images. Geometric location of 300 m or better is needed to reduce feature tracking errors. For frequency, C-band SAR is preferred due to the high radar contrast between first-year, multiyear, and wind-roughened open water, which improves feature tracking. One caveat is that the Lagrangian tracking approach used to obtain ice age places high demand on successful and regular repeating mappings. If an 'ice particle' is not imaged every 3 or 6 days, a time step uncertainty is imparted that particularly affects new ice and ridged ice production. In fact, a time gap of more than 15 days requires that a grid cell be stopped and not propagated or reinitialized with a new grid cell at a later time.

The characteristics of the ENVISAT ASAR wide swath image mode provides excellent compatibility with the RGPS input image requirements, including frequency and resolution. The 400 km swath enables nearly 100% mapping of the Arctic basin every 3-days or 12 mappings every 35-day orbit repeat cycle. Several key calibration parameters will be improvements on the RADARSAT data quality and should likewise improve the RGPS output quality. These include absolute location accuracy due to 2 pixels (150 m) and radiometric error of 0.2 dB. Also, the availability of strip map will reduce data manipulation requirements within the RGPS. The RGPS would ingest ASAR Level 1 image data and make the output products globally available. With dedicated and long-term mappings, this Arctic data would enable monitoring of the climatic changes of the Arctic sea ice cover.

CONCLUSIONS

From Arctic Ocean SAR mappings provided to date by the RADARSAT ScanSAR mode, a geophysical processor system has been developed to make the data-derived estimates of ice age and thickness for the first time ever. Continuing such mappings with ENVISAT ASAR wide swath mode would enable these critical observations of the sea ice cover to continue during a time of significant climate change that is presently taking place in the Arctic.

ACKNOWLEDGMENTS

The RADARSAT imagery is provided by the Alaska SAR Facility, Fairbanks, AK. R. Kwok and B. Holt performed this work at the Jet Propulsion Laboratory, California Institute of Technology under contract with the National Aeronautics and Space Administration.

REFERENCES

- Ingram, W. J., C. A. Wilson, and J. F. B. Mitchell, Modeling climate change: An assessment of sea ice surface albedo feedbacks, *J. Geophys. Res.*, 94, 8690-8622, 1989.
- Kattenberg, A., F. Giorgi, H. Grassl, G. A. Meehl, J. F. B. Mitchell, R. J. Stouffer, T. Tokioka, A. J. Weaver, and T. M. L. Wigley. Climate models: Projections of Future Climate. In: J. T. Houghton, L. G. Miera Filho, B. A. Callander, N. Harris, A. Kattenberg, and K. Maskell, eds., *Climate Change 1995*, Cambridge, 285-357, 1996.
- Kwok, R., D. A. Rothrock, H. L. Stern and G. F. Cunningham, Determination of Ice Age using Lagrangian Observations of Ice Motion, *IEEE Trans. Geosci. Remote Sens.*, Vol. 33(2), 392-400, 1995.
- Kwok, R. The RADARSAT Geophysical Processor System, in *Analysis of SAR data of the Polar Oceans: Recent Advances*, Tsatsoulis, C. and R. Kwok, Eds., Springer-Verlag, 235-258, 1998.
- Kwok, R. and D. A. Rothrock, Variability of Fram Strait Flux and North Atlantic Oscillation, *J. Geophys. Res.*, 104(C3), 5177-5189, 1999.
- Kwok, R. Recent changes in the Arctic Ocean sea ice circulation associated with the NAO, *Geophys. Res. Lett.*, in press.
- Maykut, G. A., The Surface Heat and Mass Balance, in *Geophysics of Sea Ice*, Ed. N. Untersteiner, 395-463, Series B: Physics Vol. 146, Plenum Press, 1986.
- Morison, J. H., M. Steele, and R. Andersen, 1998: Hydrography of the upper Arctic Ocean measured from the nuclear submarine USS Pargo. *Deep Sea Res.*, 45, 15-38.
- Parkinson, C. L., D. J. Cavalieri, P. Gloersen, H. J. Zwally, and J. Comiso, Arctic sea ice extents, areas, and trends, 1978-1996, *J. Geophys. Res.*, 104(C9), 20837-20856, 1999.
- Parmerter, R. R. and M. Coon, Model of pressure ridge formation in sea ice, *J. Geophys. Res.*, 77, 6565-6575, 1972.
- Proshutinsky, A. Y. and M. A. Johnson, Two circulation regimes of the wind-driven Arctic Ocean, *J. Geophys. Res.*, 102, 12,493-12,514, 1997.
- Rind, D., R. Healy, C. Parkinson, and D. Martinson, The role of sea ice in 2xCO₂ climate model sensitivity. Part I: The total influence of sea ice thickness and extent, *J. Climate*, 8, 449-463, 1995.
- Steele, M. and T. Boyd, Retreat of the cold halocline layer in the Arctic Ocean, *J. Geophys. Res.* 103(55), 10,419-10,435, 1998.
- Walsh, J. E., W. L. Chapman, and T.L. Shy, 1996: Recent decrease of sea level pressure in the central Arctic. Notes and Correspondence, *J. Climate*, 9, 480-486.
- Winebrenner, D. P., D. G. Long and B. Holt, Mapping the progression of melt onset and freeze-up on Arctic sea ice using SAR and scatterometry, in *Analysis of SAR data of the Polar Oceans: Recent Advances*, Tsatsoulis, C. and R. Kwok, Eds., Springer-Verlag, 129-144, 1998.
- Zhang, J., D. Rothrock, and M. Steele, Warming of the Arctic Ocean by a strengthened Atlantic inflow: Model results, *Geophys. Res. Lett.*, 25, 1745-1748, 1998.